

Sialic acid is a critical fetal defense against maternal complement attack

Markus Abeln, ... , Anja Münster-Kühnel, Birgit Weinhold

J Clin Invest. 2018. <https://doi.org/10.1172/JCI99945>.

Research In-Press Preview Immunology Reproductive biology

The negatively charged sugar sialic acid (Sia) occupies the outermost position in the bulk of cell surface glycans. Lack of sialylated glycans due to genetic ablation of the Sia activating enzyme CMP-sialic acid synthase (CMAS) resulted in embryonic lethality around day 9.5 post coitum (E9.5) in mice. Developmental failure was caused by complement activation on trophoblasts in *Cmas^{-/-}* implants accompanied by infiltration of maternal neutrophils at the fetal-maternal interface, intrauterine growth restriction, impaired placental development and a thickened Reichert's membrane. This phenotype, which shared features with complement-receptor-1 related protein Y (Crry) depletion, was rescued in E8.5 *Cmas^{-/-}* mice upon injection of cobra venom factor resulting in exhaustion of the maternal complement component C3. Here we show that Sia is dispensable for early development of the embryo proper, but pivotal for fetal-maternal immune homeostasis during pregnancy, i.e. for protecting the allograft implant against attack by the maternal innate immune system. Finally, embryos devoid of cell surface sialylation suffered from malnutrition due to inadequate placentation as secondary effect.

Find the latest version:

<https://jci.me/99945/pdf>



1 **Sialic acid is a critical fetal defense against maternal complement attack**

2 Markus Abel¹, Iris Albers¹, Ulrike Peters-Bernard¹, Kerstin Flächsig-Schulz¹, Elina Kats¹, Andreas Kispert², Stephen
3 Tomlinson³, Rita Gerady-Schahn¹, Anja Münster-Kühnel¹, Birgit Weinhold¹

4 ¹Institut for Clinical Biochemistry, Hannover Medical School, 30625 Hannover, Germany

5 ²Institut for Molecular Biology, Hannover Medical School, 30625 Hannover, Germany

6 ³Department of Microbiology and Immunology, Children's Research Institute, Medical University of South
7 Carolina, Charleston, SC 29425, USA

8

9 The authors have declared that no conflict of interest exists.

10

11 Corresponding authors:

12 Birgit Weinhold, Institut für Klinische Biochemie, Medizinische Hochschule Hannover, Carl-Neuberg-Strasse 1,
13 30625 Hannover, Germany

14 Phone: +49511-5323947

15 Weinhold.Birgit@mh-hannover.de

16

17 Anja Münster-Kühnel, Institut für Klinische Biochemie, Medizinische Hochschule Hannover, Carl-Neuberg-Strasse
18 1, 30625 Hannover, Germany

19 Phone: +49511-5323947

20 Muenster.Anja@mh-hannover.de

21

22 **Abstract:**

23 The negatively charged sugar sialic acid (Sia) occupies the outermost position in the bulk of cell surface glycans.
24 Lack of sialylated glycans due to genetic ablation of the Sia activating enzyme CMP-sialic acid synthase (CMAS)
25 resulted in embryonic lethality around day 9.5 post coitum (E9.5) in mice. Developmental failure was caused by
26 complement activation on trophoblasts in *Cmas*^{-/-} implants accompanied by infiltration of maternal neutrophils at
27 the fetal-maternal interface, intrauterine growth restriction, impaired placental development and a thickened
28 Reichert's membrane. This phenotype, which shared features with complement-receptor-1 related protein Y
29 (Crry) depletion, was rescued in E8.5 *Cmas*^{-/-} mice upon injection of cobra venom factor resulting in exhaustion of
30 the maternal complement component C3. Here we show that Sia is dispensable for early development of the
31 embryo proper, but pivotal for fetal-maternal immune homeostasis during pregnancy, i.e. for protecting the
32 allograft implant against attack by the maternal innate immune system. Finally, embryos devoid of cell surface
33 sialylation suffered from malnutrition due to inadequate placentation as secondary effect.

34

35 **INTRODUCTION**

36 Every living cell is coated with a dense layer of glycans, the glycocalyx. In mammals, ten different
37 monosaccharides can be assembled in various linkages, generating an enormous number of glycans, encoding a
38 vast amount of information which is utilized in cellular communication (1). Moreover, glycosylation of proteins
39 and lipids is cell-type-specific and influenced by e.g. metabolic state, differentiation and environmental factors
40 (2). Although recent advances in glycoanalytical technologies now shed light on specific glycosylation patterns and
41 identify disease-associated alterations, many structure-function relationships still await elucidation (3). A sugar
42 known to have a major impact on the functions of glycans is the negatively charged nonulose sialic acid (Sia). Sia is
43 situated at the terminal position of a multitude of glycan structures, thus shaping the outermost identity of a cell.
44 It is therefore not surprising that Sia modulates central cellular functions such as cell-cell communication, signal
45 transduction, and cell migration (3,4). Moreover, Sia can dampen immune responses by acting as a ligand for Sia-
46 binding immunoglobulin-like lectins (Siglecs), predominantly found on immune cells, and the complement
47 regulating fluid-phase protein factor H (5,6). Hence, Sia is recognized as self-associated molecular patterns
48 (SAMP), promoting discrimination between self and non-self (7). Sialylation in mammals occurs in either α 2,3- or
49 α 2,6-glycosidic linkage to the underlying sugar galactose or *N*-acetylgalactosamine, or in an α 2,8-linkage when
50 two or more Sia residues are linked to another in di-, oligo- or polysialylated glycans by Golgi-resident
51 sialyltransferases. All sialyltransferases strictly depend on the preceding activation of Sia to CMP-Sia, which is
52 catalysed by the nuclear localised enzyme CMP-sialic acid synthase (CMAS) (8). We have recently shown that
53 genetic inactivation of the *Cmas* gene results in loss of CMAS protein and complete lack of sialoglycans on the cell
54 surface of murine embryonic stem cells (mESC) (9). Fully unexpectedly, the asialo mESC were equivalent to
55 control mESC in terms of differentiation, indicating that Sia is dispensable for germ layer formation and early
56 embryonic development in vitro. In accord with our observations, a mouse model deficient in the first committed
57 enzyme in the Sia de novo biosynthesis, the bifunctional enzyme UDP-*N*-acetylglucosamine 2-epimerase/*N*-
58 acetylmannosamine kinase (GNE), is embryonic lethal around E9.5, a time point when all germ layers have formed
59 (10). Nevertheless, the embryonic lethal GNE phenotype highlights the substantial importance of Sia for
60 mammalian development.

61 In eutherian pregnancy exact orchestration of signalling events and precise immune homeostasis are crucial for
62 proper development and survival of the fetus (11). During early pregnancy, the blastocyst stage embryo is
63 subdivided into the inner cell mass, giving rise to the embryo proper, and the trophoblast layer, forming
64 extraembryonic tissues from which amongst others the future placenta derives (12). However, also the inner cell
65 mass contributes to the generation of extraembryonic tissues by forming the Reichert's membrane and the
66 visceral endoderm, which ensure fetal nourishment during early development until blood flow through the
67 placenta is properly established at E14.5 in mice (13-15). Evolution established different types of placentation in
68 mammals. Mice and humans both form a hemochorial placenta, in which the maternal blood passes through
69 vascular spaces with fetal trophoblast cells, rather than maternal endothelial cells forming the vascular barrier
70 (16). Consequently, the extraembryonic components of the developing fetus are in direct contact to maternal
71 blood. This is a challenging situation since the embryo bears paternal antigens and is a semi-allograft to its
72 mother. Thus, fetal trophoblasts in hemochorial placentae are particularly vulnerable and in need of preventing
73 an immune attack at the fetal-maternal interface. Numerous immune protective mechanisms have evolved to
74 fulfil this task. On the fetal side for instance, trophoblasts express a distinct subset of MHC molecules that seem
75 to promote maternal immune tolerance of fetal tissues (17-19). Additionally, multiple complement regulatory
76 proteins (CD55, CD46, CD59 and Crry) are expressed on fetal trophoblasts and control first line immune defence
77 mechanisms (20,21). On the maternal side, the decidua protects the developing embryo by limiting access of
78 maternal T- and B-cells to the implant (22,23). Dysregulation of immune homeostasis during pregnancy can lead
79 to severe complications, such as recurrent pregnancy loss or preeclampsia. The latter affects 2-8% of pregnancies

80 worldwide and patients show placental deficits and intrauterine growth restriction, hence posing a severe threat
81 for mother and fetus (24-26).

82 Although Sia is known for long as pivotal for embryonic development and involved in immunoregulation, its
83 precise functions and its role in the interplay between immune protection and embryonic development in
84 mammals is not understood so far. Here, we demonstrate that sialylation is less important for early
85 developmental steps of the embryo proper, but is crucial for maintenance of immune-homeostasis at the fetal-
86 maternal interface. Trophoblasts were extensively sialylated in the wildtype, but did not express Sia in *Cmas*^{-/-}
87 embryos. As a consequence immune-protection failed and the maternal complement system attacked
88 extraembryonic tissues resulting in defective placentation, intrauterine growth restriction and ultimately fetal
89 demise.

90 **RESULTS**91 **Depletion of CMAS leads to loss of sialoglycoconjugates in *Cmas*^{-/-} embryos and is embryonic lethal**

92 Genetic inactivation of *Cmas* in mice was accomplished as described by excision of exon 4, which encodes
 93 residues essential for enzymatic activity (9). All genotypes of offspring from *Cmas*^{+/+} intercrosses were discovered
 94 in Mendelian ratio until E8.5 (Figure S1). *Cmas*^{-/-} embryos were observed only very rarely between E9 and E10 and
 95 were never born. *Cmas* heterozygous mice were indistinguishable from wildtype. To evaluate the sialylation
 96 pattern in control and *Cmas*^{-/-} E6.5 and E8.5 implants, paraffin sections from uteri of pregnant *Cmas*^{+/+} female
 97 (bred to *Cmas*^{+/+} males) were stained with *Maackia amurensis* agglutinin (MAA), which binds to α2,3-linked sialic
 98 acids on glycans (Figure 1A). Simultaneously, the same sections were probed with peanut agglutinin (PNA) lectin,
 99 detecting galactose as terminal sugar (27). Since under normal conditions the bulk of galactose residues is capped
 100 with Sia, PNA staining becomes prominent in the absence of Sia (Figure 1A). In E6.5 control animals, MAA
 101 reactivity was prominent on the surface of trophoblast cells at the ectoplacental cone (EPC), on trophoblast giant
 102 cells (TGC) lining the fetal-maternal interface (arrowheads) and on the apical side of the embryonic and
 103 extraembryonic ectoderm facing the proamniotic cavity (arrow) (Figure 1B). Notably, apart from the observed
 104 reactivity at the apical side of the embryonic ectoderm, the embryo proper did not exhibit MAA reactivity. At
 105 E8.5, MAA reactivity at the EPC and on TGC became even more pronounced and could also be observed on the
 106 Reichert's membrane (asterisk), head mesenchymal cells (arrowheads) and the apical side of fetal epithelia
 107 (arrows) in control animals. TGC identity of MAA positive cells at the fetal-maternal interface of control implants
 108 was verified by co-staining of MAA and the trophoblast marker cytokeratin-8 (Figure S2A). Consistent with *Cmas*^{-/-}
 109 mESC, E6.5 as well as E8.5 *Cmas*^{-/-} embryonic and extraembryonic tissues were devoid of α2,3-linked sialic acids as
 110 visualized by lack of MAA staining. The MAA positive cells in the vicinity of *Cmas* negative TGCs have been
 111 identified as maternal granulocytes (Figure S2B). To confirm the loss of Sia on glycans and in order to detect
 112 terminal galactose residues, uteri sections were simultaneously probed with PNA. Control animals showed slight
 113 PNA reactivity at the apical side of epithelia at E6.5 and E8.5 (Figure 1B, arrows), whereas *Cmas*^{-/-} tissue was
 114 highly PNA positive with particularly intense staining in the trophoblast layer and at the apical side of visceral
 115 endoderm cells at both analysed time points. Hence, loss of terminal Sia resulted in concomitant appearance of
 116 underlying galactosyl residues on the cell surface of *Cmas*^{-/-} embryonic and extraembryonic tissues. Interestingly,
 117 the PNA staining in *Cmas*^{-/-} trophoblasts resembled the pattern of MAA staining in control animals, suggesting
 118 that most of the PNA epitopes on control trophoblasts were capped with α2,3-linked sialic acids. Specificity of the
 119 MAA reactivity for Sia was confirmed by enzymatic removal of Sia by neuraminidase treatment of the sections
 120 prior to incubation with the lectins. As expected, neuraminidase treatment abolished MAA staining in control
 121 animals and gave rise to PNA staining on trophoblasts, embryonic epithelia and mesenchymal cells.
 122 Neuraminidase treated *Cmas*^{-/-} tissues did not show any difference in MAA or PNA reactivity compared to
 123 untreated samples of the same genotype (Figure 1B). Visualisation of α2,6-linked sialic acids was accomplished by
 124 detection with *Sambucus nigra* agglutinin (SNA). SNA reactivity was prominent on the cell surface of embryonic
 125 ectodermal cells (arrow) as well as on amniotic and allantoic cells in control embryos (Figure S3). In addition, TGCs
 126 showed an intracellular staining for SNA. *Cmas*^{-/-} implants lacked cell surface SNA reactivity of the aforementioned
 127 tissues, but like wildtype displayed the intracellular SNA staining in TGCs, which most likely reflects endocytosed
 128 material of maternal origin. The Sia specificity of the lectin was again demonstrated by complete loss of SNA
 129 reactivity and an increase in PNA epitopes upon enzymatic removal of Sia by neuraminidase treatment prior to
 130 lectin incubation. The simultaneous lack of MAA and SNA reactivity and the presence of PNA binding sites in
 131 knockout embryos confirmed that loss of CMAS activity resulted in a complete lack of cell surface sialylation
 132 referred to as asialo phenotype, identical to the situation in *Cmas*^{-/-} mESCs (9).

133 **Loss of CMAS results in intrauterine growth restriction**

134 To follow up embryonic development hematoxylin and eosin stained sections of uteri were assessed. At E6.5 the
 135 morphology of embryonic ectoderm (EC) and extraembryonic ectoderm, visceral endoderm (VE) and the
 136 proamniotic cavity (PC) was indistinguishable between *Cmas*^{-/-} and control implants (Figure 2A). At E7.5 the three
 137 germlayers ectoderm, endoderm, and mesoderm (ME) had been established in control as well as *Cmas*^{-/-}
 138 embryos. Mesodermal cells could be observed migrating from the primitive streak to the anterior part of the
 139 embryo in both genotypes (Figure 2A, insets). At E8.5, *Cmas*^{-/-} mice were characterised by a marked variability in
 140 developmental deficits. Some embryos formed somites (S), the heart (H) and showed neurulation, whereas others
 141 were considerably less well-structured or consisted of a widely unstructured agglomeration of cells (Figure 2A and
 142 S4A). Phenotypic variability was also reflected by heterogeneous organisation of mesodermal structures, which
 143 we monitored by *in situ* hybridisation analysis of the major mesoderm regulator *Brachyury*. *Brachyury* was
 144 localised at the primitive streak in control animals but was either irregularly distributed or ectopically expressed
 145 in numerous *Cmas*^{-/-} embryos (Figure S4B). To quantify the fetal growth between E6.5 and E8.5, the combined
 146 total area of amniotic cavity, exocoelomic cavity, ectoplacental cavity and embryo proper was measured on
 147 sagittal sections. A schematic overview is depicted in Figure S5. At E6.5 no significant differences in fetal growth
 148 were observed (Figure 2B). At E7.5, *Cmas*^{-/-} mice showed only 52% ($p = 0.045$) of the size of control animals
 149 (*Cmas*^{+/+} or *Cmas*⁺⁺). Intrauterine growth restriction (IUGR) increased with progression of pregnancy at E8.5,
 150 where *Cmas*^{-/-} embryos reached only 36% ($p = 0.029$) of the size of controls. Taken together, loss of sialylation did
 151 not impair morphogenesis and differentiation processes in the embryo proper of *Cmas*^{-/-} mice until E7.5, although
 152 already a significant IUGR was observed. Growth restriction affected all *Cmas*^{-/-} embryos at E8.5 and development
 153 of the embryo proper was at this time point characterized by a large variability, ranging from proper formation of
 154 e.g. somites up to embryos with extensive loss of developmental orchestration.

155 *Cmas*^{-/-} mice exhibit severe extraembryonic defects

156 The pronounced IUGR in *Cmas*^{-/-} animals together with a broad heterogeneity in the development of the embryo
 157 proper suggested a contribution of deficits in extraembryonic tissues. These tissues (e.g. visceral endoderm,
 158 amnion and trophoblasts) are embryonic derivatives that do mostly not contribute to the later animal but are
 159 essential for fetal nourishment, waste exchange, and protection. We first analysed the structure of the
 160 ectoplacental cone (EPC) and the chorionic plate (CP). Both structures harbour trophoblast stem cells, which give
 161 rise to different cell types of the later placenta (28). The EPC however is in direct contact with the maternal
 162 decidua, whereas the CP is located inside the fetal compartment at the mesometrial side of the exocoelomic
 163 cavity. Trophoblasts are characterized by expression of the intermediate filament cytokeratin-8 that could
 164 immunohistochemically be detected by the TROMA-I antibody on trophoblasts at the EPC and on trophoblast
 165 giant cells (TGC), which, due to their polyploid nature, are characterised by large nuclei (29) (Figure 2C). As
 166 described in literature, EPCs of control mice were properly structured at E8.5 and displayed internally localised
 167 trophoblast cells (arrowheads), which are reported to contribute to the spongiotrophoblast and labyrinth
 168 placental layer at later time points in development (28). In contrast, the EPC of *Cmas*^{-/-} animals appeared heavily
 169 disorganised. The structure was either devoid of internally localised trophoblasts or the number of trophoblasts
 170 was dramatically decreased (Figure 2C). In addition to their localization at the EPC, TGCs continuously lined the
 171 fetal-maternal interface of control mice at the site of decidual contact. Although TGCs were present in this
 172 compartment, a continuous trophoblast layer was not established at the interface of *Cmas*^{-/-} mice (Figure 2C).
 173 Importantly, the chorionic plate was properly established at E8.5 in control animals, but was absent or - in those
 174 rare cases where it could be detected in *Cmas*^{-/-} mice - was dramatically reduced in its spatial expansion (Figure 2C
 175 and Figure S4A).

176 Another tissue important for regulation of nutrient and waste exchange during the first days of gestation when in-
 177 and efflux through the placenta is not yet established, is the Reichert's membrane (RM) (30,31). The RM is the
 178 outermost basement membrane deposited by cells of the parietal endoderm (extraembryonic tissue) and
 179 characterized by collagen IV and laminin expression. Staining of both markers in control mice showed a thin and

180 well-structured RM with a monolayer of parietal endoderm cells situated like pearls on a string on top, whereas
 181 *Cmas*^{-/-} mice exhibited tremendous deposition of collagen IV and laminin at the RM accompanied by accumulation
 182 of parietal endodermal cells at the antimesometrial pole at E.8.5 (Figure 2D).

183 In sum, loss of sialylation led to the appearance of severe extraembryonic defects, which all are likely to
 184 contribute to the observed growth restriction of *Cmas*^{-/-} embryos.

185 **The fetal-maternal interface of *Cmas*^{-/-} mice is infiltrated with maternal neutrophils**

186 The detailed analysis of trophoblasts and the RM revealed that the fetal-maternal interface of *Cmas*^{-/-} mice was
 187 tremendously infiltrated with polymorphonuclear leukocytes, indicating a major inflammation at the site of
 188 implantation. To investigate the immunological situation in more detail, we analysed the presence of different
 189 leukocyte populations in the decidua of *Cmas*^{-/-} and control animals over time (E6.5 to E8.5). Both, neutrophils
 190 and monocytes are characterised by the granulocyte receptor-1 (Gr-1) epitope, but neutrophils can
 191 morphologically be distinguished from monocytes by segmented nuclei. At all analysed time points, Gr-1 positive
 192 cells in control mice were rare and their presence predominantly restricted to the site of contact between the EPC
 193 and the decidua (Figure 3A). However, in deciduae of *Cmas*^{-/-} embryos numbers of Gr-1 positive cells were already
 194 significantly elevated up to 6-fold ($p = 0.002$) at E6.5. This increase was maintained at E7.5 ($p = 0.0001$) and
 195 dramatically augmented at E8.5 ($p = 0.002$), when the entire implantation site of *Cmas*^{-/-} embryos was infiltrated
 196 with maternal neutrophils. Neutrophil identity of Gr-1 positive cells in the deciduae was verified by staining of the
 197 neutrophil specific epitope Ly6G (Figure S6). Under normal conditions, the most abundant decidual leukocyte
 198 population are decidual NK (dNK) cells, which play an important role during vascularisation and in immune
 199 surveillance in the decidua (32). dNK cells are characterized by glycoprotein rich cytoplasmic granules containing
 200 α -linked N-acetylgalactosamine, a sugar moiety that can be recognized by *Dolichus biflorus* lectin (DBA) (33). The
 201 localisation of DBA positive dNK cells was comparable in control and *Cmas*^{-/-} implants from E6.5 to E8.5. Similarly,
 202 the number of DBA positive cells in the decidua basalis did not differ significantly (E6.5: $p = 0.77$; E7.5: $p = 0.112$;
 203 E8.5: $p = 0.865$) between *Cmas*^{-/-} and controls (Figure 3B). Likewise, the number of decidual macrophages,
 204 identified by immunohistochemical staining of the marker F4/80, although increased at E8.5, did not deviate
 205 significantly between *Cmas*^{-/-} and controls in the analysed time frame (E6.5 $p = 0.678$; E7.5 $p = 0.532$; E8.5 $p =$
 206 0.188) (Figure 3C). We conclude that maternal neutrophils, but not decidual macrophages or dNK cells, infiltrated
 207 the fetal-maternal interface of *Cmas*^{-/-} implants as early as E6.5, i.e. prior to morphological defects of *Cmas*^{-/-}
 208 embryos.

209 **Depletion of maternal neutrophils does not ameliorate the *Cmas*^{-/-} phenotype**

210 Neutrophil infiltration of the fetal-maternal interface has previously been described to contribute to fetal demise
 211 in inflammation related mouse models of recurrent pregnancy loss (24). With the aim to rescue a putative
 212 neutrophil driven inflammation and to attenuate the *Cmas*^{-/-} phenotype, we injected the neutrophil specific anti-
 213 Ly6G antibody into *Cmas*^{-/-} pregnant mice at day E4.5 as previously described by Daley et al. (34). To validate the
 214 absence of neutrophils in the maternal circulation after antibody treatment, maternal whole blood was analysed
 215 for Ly6G positive cells at day E8.5 by FACS analysis. The blood of untreated *Cmas*^{-/-} mice harboured a distinct Ly6G
 216 positive population, which was successfully depleted in anti-Ly6G injected mice (Figure 4A). In line with depletion
 217 of neutrophils in the maternal circulation, also the prominent infiltration of *Cmas*^{-/-} implants with maternal
 218 neutrophils was abolished at E8.5 (Figure 4B). However, despite the fact that neutrophilia was abrogated, *Cmas*^{-/-}
 219 embryos still revealed a significant IUGR ($p = 0.0012$) similar to *Cmas*^{-/-} embryos of untreated mothers (Figure 4C,
 220 Figure 2B). Moreover, the deficits in placental development, as can be seen by TGC malformation and loss of
 221 trophoblast cells at the CP and EPC, were equivalent to *Cmas*^{-/-} implants of untreated pregnant mice (Figure 4D).
 222 Also, the RM of *Cmas*^{-/-} implants in neutrophil depleted mothers was still thickened and comparable to the RM of
 223 *Cmas*^{-/-} implants of untreated mothers (Figure 4E). Taken together, these data demonstrate that the presence of
 224 maternal neutrophils was not causative for the observed embryonic and extraembryonic defects in *Cmas*^{-/-} mice.

225 **Maternal complement attack causes the *Cmas*^{-/-} phenotype**

226 Similar to humans, mice form a hemochorial type of placenta in which the maternal blood is in direct contact with
 227 fetal trophoblast cells (11). Hence, also humoral and complement components interact directly with fetal cells
 228 and their dysregulation is associated with pregnancy complications (35). To elucidate if activation of the maternal
 229 complement system is involved in the loss of fetal-maternal immune homeostasis in *Cmas*^{-/-} pregnancies, we
 230 analysed the deposition of the central complement component 3 (C3) at E8.5. All implants, irrespective of their
 231 genotypes, revealed C3 staining at the interface between EPC and decidual stroma (Figure 5A). Apart from this, no
 232 C3 deposition was observed at the fetal-maternal border of control implants. In sharp contrast, C3 staining was
 233 observed along the entire fetal-maternal interface in *Cmas*^{-/-} embryos. Especially TGCs exhibited strong C3
 234 staining on their cell surface, suggesting an increased activation of the maternal complement system, whereas
 235 TGCs of control mice were devoid of C3 on the cell surface (Figure 5A, insets). In addition, control animals
 236 exhibited a prominent intracellular staining of C3 in the VE (Figure 5A, arrows), which was mostly absent in *Cmas*
 237 ^{-/-} implants. Differences in C3 deposition also occurred in mice that were depleted from maternal neutrophils,
 238 indicating that loss of neutrophils did not prevent complement activation on *Cmas*^{-/-} TGCs (Figure 5B).

239 To evaluate whether the increased complement activation on fetal trophoblasts of *Cmas*^{-/-} embryos evoked the
 240 phenotype of *Cmas*^{-/-} implants, pregnant mice were injected with cobra venom factor (CVF) at E4.5 and E6.5.
 241 Along with serum proteins CVF forms a stable C3 convertase and exhausts C3 from the circulation. This technique
 242 has been successfully applied in various studies to deplete mice (36). Depletion of C3 in CVF treated
 243 animals was verified by Western blot analysis of sera isolated from PBS and CVF injected pregnant mice at E8.5
 244 (Figure 6A). In *Cmas*^{-/-} implants CVF injection reverted C3 deposition on TGCs (Figure 6B) and simultaneously
 245 reduced the number of maternal neutrophils at the fetal-maternal interface ($p < 0.001$) (Figure 6C and D). After
 246 CVF treatment C3 deposits as well as macrophage and neutrophil ($p > 0.05$) numbers were comparable in
 247 knockout and control implants (Figure S7).

248 Next, we analysed if C3 depletion also rescues the defects observed in extraembryonic tissue of *Cmas*^{-/-} embryos.
 249 Of note, as visualised by cytokeratin-8 staining, *Cmas*^{-/-} implants of CVF treated females revealed a continuous
 250 layer of TGCs, as well as a restored EPC and CP indistinguishable from control implants in the same uterus (Figure
 251 7A). To exclude the possibility that CVF treatment per se may alter embryonic or extraembryonic development,
 252 we carefully controlled wildtype implants isolated from CVF treated heterozygous dams with implants isolated
 253 from CVF treated and untreated wildtype dams. At histological level no sign of aberrant development induced by
 254 CVF could be identified.

255 The integrity of the CP in *Cmas*^{-/-} embryos was addressed by analysing the expression of the CP marker
 256 CCAAT/enhancer binding protein- β (Cebpb), a transcription factor involved in placental vascularization (37,38).
 257 Cebpb was strongly expressed in the CP of control animals at E8.5 but almost absent in *Cmas*^{-/-} CP (Figure 7A, PBS
 258 treated mice). Importantly, the Cebpb pattern in *Cmas*^{-/-} implants was re-established upon CVF treatment,
 259 strongly suggesting that the CP was not only morphologically but also functionally restored (Figure 7A, CVF
 260 treated mice). CVF rescued *Cmas*^{-/-} embryos maintained PNA reactivity on TGCs and other fetal trophoblast cells
 261 at the EPC, confirming their asialo nature equivalent to *Cmas*^{-/-} embryos of untreated mothers (Figure 7A).

262 Beyond restoring trophoblast development, the maternal decompensation also significantly decreased the
 263 thickness of the RM in *Cmas*^{-/-} implants ($p < 0.001$) (Figure 7B and C), fully compensated the IUGR of *Cmas*^{-/-}
 264 embryos ($p < 0.05$) (Figure 7D) and abrogated phenotypic variability of the embryo proper (Figure S8).

265 This experimental series clearly demonstrated that depletion of complement factor C3 by CVF treatment was
 266 sufficient to completely rescue the observed extraembryonic deficits as well as IUGR at E8.5 of *Cmas*^{-/-} mice.

267 **Loss of sialic acid activates the alternative complement pathway on the surface of TGCs**

268 Activation of the complement cascade occurs through three major pathways, the classical, the lectin and the
269 alternative pathway. To delineate which pathway is involved in the emergence of the *Cmas*^{-/-} phenotype we
270 analysed the presence of respective complement pathway marker proteins. The classical pathway is initiated by
271 binding of antibodies to the cell surface and subsequent recognition of bound antibodies by C1q complexes.
272 Neither control, nor *Cmas* negative trophoblasts were positive for C1q (Figure 8A). The classical and the lectin
273 pathway both include cleavage of C4, making C4d a prevalently used marker for detection of classical and lectin
274 pathway activation (39). C4d reactivity was observed in the maternal stroma adjacent to the EPC, but TGCs did
275 not show any C4d staining in control or *Cmas*^{-/-} implants (Figure 8B). The alternative complement pathway
276 convertase C3bBb is stabilised by the fluid-phase component properdin (40). Similar to C3 deposition, properdin
277 staining was absent on control trophoblasts, but very prominent on *Cmas*-negative TGCs, strongly indicating
278 involvement of the alternative pathway (Figure 8C). Finally, we interrogated if complement activation results in
279 formation of the membrane attack complex (MAC) and stained for the presence of the MAC component C9.
280 However, no reactivity for C9 could be observed (Figure 8D).

281

282 **DISCUSSION**

283 Fetal development inside the womb has many benefits, a few of which are protection from fluctuations in
 284 nourishment, temperature and oxygen levels (41). Beyond the safety from external threats, fetal in utero
 285 existence however entails problems. Among the biggest challenges for mother and fetus is the establishment of
 286 immunologic coexistence of two genetically distinct entities, while simultaneously ensuring potent immune
 287 defense against pathogens. To date, several maternal and fetal mechanisms contributing to the establishment
 288 and maintenance of fetal-maternal immune homeostasis have been described (11). Yet, numerous non pathogen-
 289 related inflammatory reactions leading to pregnancy complications exist, which represent major threats to the
 290 developing fetus and its mother (42). Using a CMP-sialic acid negative mouse model, we demonstrated sialylation
 291 to be crucial for protection of fetal extraembryonic tissue from maternal complement attack, thereby
 292 guaranteeing its proper development which ultimately ensures adequate nourishment of the embryo proper.

293 The abundance of sialic acids and their outermost location on vertebrate cell surfaces enables sialoglycans to
 294 execute a myriad of functions, ranging from more global physicochemical functions to specific receptor-ligand
 295 mediated interactions (43). 15 years have passed since Horstkorte and colleagues showed genetic disruption of
 296 sialic acid de novo synthesis to cause embryonic lethality at E9.5 in mice (10). However, until today studies
 297 interrogating the underlying mechanisms are missing and little is known about the occurrence and functions of
 298 sialoglycans during embryonic development. MAA lectin analyses carried out in the current study revealed that
 299 α 2,3-linked sialic acids were only sparsely found in the pre-streak embryo (E6.5), but were abundant on the cell
 300 surface of extraembryonic trophoblasts. This pattern was maintained for E8.5 implants with slight increase in the
 301 embryo proper (e.g. on ectodermal cells) and prominent staining in extraembryonic compartments, i.e.
 302 trophoblasts at the fetal-maternal interface. α 2,3-linked sialic acids have also been described to be present on
 303 human trophoblasts facing the maternal blood or invading the maternal decidua, potentially indicating a similar
 304 function of α 2,3-sialylation in different species with hemochorial placentation (44). Loss of CMAS in mice,
 305 however, was accompanied by a complete lack of MAA reactivity at all analysed time points. α 2,6-linked sialic
 306 acids in control implants were prominent on embryonic ectoderm, amniotic and allantoic cells. Equivalent to
 307 α 2,3-linked sialic acids, *Cmas*^{-/-} embryos also revealed a lack of α 2,6-sialylated glycans. Interestingly, control as
 308 well as *Cmas*^{-/-} TGCs showed neuraminidase sensitive intracellular SNA staining. Since previous studies clearly
 309 demonstrated that loss of CMAS causes an asialo phenotype in embryonic stem cells in vitro and trophoblast cells
 310 are known to endocytose certain maternal proteins, e.g. immunoglobulins, the observed intracellular SNA
 311 reactivity in TGCs most likely represented internalised maternal material (9,45). Most notably, asialo *Cmas*^{-/-}
 312 embryos established neuroepithelia, head mesenchyme as well as heart primordia and somites, promoting the
 313 hypothesis that sialoglycans are mostly dispensable for development of the embryo proper until E8.5. Although
 314 only few sialylated structures were detected with MAA in control embryos, this result was unexpected, also
 315 because the apical domain of the embryonic ectoderm showed unequivocal presence of α 2,3-linked sialic acid
 316 already at E6.5. Moreover, previous reports postulated that sialylation of the apical domain of the embryonic
 317 ectoderm might contribute to the formation of the proamniotic cavity lumen by charge repulsion (46). Based on
 318 our current observation that all *Cmas*^{-/-} mice have formed a proper proamniotic cavity by E6.5, the establishment
 319 of this lumen does apparently not exclusively rely on charge repulsion by sialoglycans but includes additional
 320 mechanisms.

321 Despite the large heterogeneity in embryonic development of E8.5 *Cmas*^{-/-} epiblasts, all *Cmas*^{-/-} implants featured
 322 a substantial IUGR, severe deficits in placental development and a thickened RM. The simultaneous extensive
 323 infiltration of maternal neutrophils into the fetal-maternal interface and increased deposition of C3 components
 324 favour the assumption that disturbance of the fetal-maternal immune homeostasis accounts for these phenotypic
 325 abnormalities. The decidua generates an immunologically privileged environment for the developing fetus by
 326 preventing the entry of certain types of leukocytes. B- and T-cells are prominent in the maternal blood but their
 327 numbers are drastically reduced in the pregnant decidua. Furthermore, decidual stromal cells are able to silence

328 the expression of chemokine genes needed for invasion of effector T-cells (22,23). As a consequence, the adaptive
329 immune system is largely excluded from access to fetal tissue from early to mid-pregnancy. With some
330 exceptions, this does not apply to the maternal innate immune system which is in direct contact with fetal
331 trophoblasts at the EPC and TGCs.

332 It has been postulated that sialoglycans on the cell surface have evolved as an important mechanism of self-
333 recognition, i.e. that Sia promotes discrimination between host tissue and pathogens (7). This immunomodulatory
334 function is inter alia established through attenuation of immune responses by Siglecs, which are expressed by a
335 wide range of adaptive and innate immune cells (5,47). Upon binding of the respective sialoglycan, some
336 members of the Siglec family negatively regulate immune responses through their immune-receptor tyrosine-
337 based inhibitory motifs (ITIM) (48;49). Murine neutrophils prominently express Siglec-E, which dampens the
338 immune response of neutrophils upon binding to α 2,3-linked sialylated glycans (50). The absence of Siglec-E
339 ligands and the most probably abrogated Siglec-E mediated control of neutrophils in *Cmas*^{-/-} trophoblasts implied
340 that an excessive immune response by maternal neutrophils could account for the disturbed development of
341 asialo trophoblasts. Even though neutrophil involvement in pregnancy complications in mice and humans is
342 described (51), this hypothesis could be refuted since depletion of maternal neutrophils did not ameliorate any of
343 the observed embryonic or extraembryonic deficits of *Cmas*^{-/-} concepti. Taking into account that Siglec-E
344 negatively influences immune responses of neutrophils also in group B *Streptococcus* and pulmonary
345 inflammations (52), Siglec-E mediated self-recognition might not apply in the context of semi-allogeneic fetal
346 trophoblasts in the absence of other proinflammatory stimuli.

347 CVF rescue experiments provided conclusive evidence that aberrant activation of the maternal complement
348 pathway was a key cause of developmental deficits in *Cmas*^{-/-} implants. Although CVF produces complement
349 activation products, e.g. C3a and C5a in the serum of treated mice (53), neither *Cmas*^{-/-} nor control littermates
350 showed any adverse effect resulting from CVF injection. The CVF mediated depletion of C3 in the maternal serum
351 abrogated excessive complement activation on asialo TGCs and at the same time restored development of the CP,
352 EPC and TGCs. Strikingly, CVF treatment also prevented excessive thickening of the RM, restored growth of *Cmas*^{-/-}
353 embryos and prevented infiltration with maternal neutrophils. Considering that neutrophils are attracted by the
354 complement cleavage products C3a and C5a, and that antibody induced depletion of neutrophils did not rescue
355 the *Cmas*^{-/-} phenotype, our data evidence that neutrophil recruitment to *Cmas*^{-/-} implants was a secondary effect
356 following excessive complement activation. This assumption probably also holds true for the slightly elevated
357 numbers of decidual macrophages, since this effect was reverted by CVF injection and macrophages have been
358 described to express anaphylotoxin receptors (54,55). Because extraembryonic tissues are crucial structures also
359 in embryonic nourishment and waste exchange, we can conclude that deficits in their development most likely
360 caused embryonic malnutrition and IUGR in *Cmas*^{-/-} implants. Moreover, the proper development of
361 extraembryonic tissues in *Cmas*^{-/-} implants after CVF treatment argues for its independence from sialylation. In
362 contrast, the establishment of the fetal-maternal immune homeostasis essentially depends on sialylation as
363 demonstrated by the rescue of the *Cmas*^{-/-} phenotype at E8.5 by complement depletion. Increased deposition of
364 C3 on asialo TGCs was indicative for excessive complement activation, but did not allow discriminating between
365 the potential pathways. C1q complexes are an essential part of classical complement pathway activation and C4d
366 reactivity is an established diagnostic marker for activation of the classical and/or lectin complement pathway
367 (39). Absence of both C1q and C4d strongly suggested that neither the classical nor the lectin pathway were
368 involved in the pathogenesis of the *Cmas*^{-/-} phenotype. Analysis of properdin, a potent stabiliser of the alternative
369 pathway C3 convertase, however revealed increased reactivity on the cell surface of *Cmas*^{-/-} TGCs (40). Taken
370 together our data suggest that loss of sialylation on TGCs involved activation of the alternative complement
371 pathway. However, increased levels of the membrane attack complex (MAC) monitored by C9 staining were not
372 seen. Hence, developmental deficits observed in *Cmas*^{-/-} extraembryonic tissues were by all likelihood not the
373 result of cellular lysis, but were the consequences of other yet to be identified complement related mechanisms.

374 Similar to *Cmas*^{-/-} implants, mice lacking the complement regulatory protein Crry exhibit a phenotype that
375 includes excessive complement activation, neutrophil recruitment to the site of implantation, and deficits in
376 placental development (56). It appears that failure or lack of one protective component, be it Sia or Crry, is
377 sufficient to unhinge regulation of the complement system, underpinning the fragility of complement regulation
378 at the fetal-maternal interface. The fact that human trophoblasts express numerous complement regulating
379 proteins, further highlights the importance of a well-orchestrated protection against the maternal complement
380 system in hemochorial placentation (20). Also noteworthy is the deposition of C3 at the EPC that was observed in
381 all analysed genotypes and has previously been reported (56). This supports the speculation that controlled
382 complement activation may be physiological in placental development, e.g. to stimulate remodelling of the fetal-
383 maternal interface at the EPC and clearance of cellular debris.

384 The mechanisms that induce activation of the alternative complement pathway in *Cmas*^{-/-} mice remain unclear.
385 One possible explanation might be an impaired function of factor H (CFH), a serum protein and negative regulator
386 of the complement cascade. Upon binding CFH destabilises existing C3 convertases and recruits factor I, which
387 cleaves C3b and thus prevents C3 convertase complex formation (57). Recently, Blaum and coworkers
388 demonstrated that efficient recruitment of CFH to the cell surface requires the presence of α2,3-sialylated glycans
389 (5). Furthermore, mutations in the *CFH* gene affecting the sialic acid recognition site have been associated with
390 the atypical haemolytic syndrome, a pathology characterised by excessive activation of the complement system
391 (5,58). However, CFH deficient mice are fertile and the complement system is intricately regulated by a multitude
392 of factors (59). Thus, the mechanisms that disequilibrated the complement system in *Cmas*^{-/-} embryos could not
393 yet be addressed in our mouse model and require further investigations. Our future work will make use of
394 conditional *Cmas* mice allowing the depletion of CMAS in a cell type specific manner (e.g. individual trophoblast
395 cell types or embryo proper) and by crossing in the C3 knockout.

396 Finally it is worth mentioning that preeclampsia, a pregnancy complication that affects 2-8% of all pregnancies,
397 involves excessive activation of the complement system and decidual inflammatory reactions, leading to placental
398 deficits, IUGR and maternal cardiovascular complications (60,61). To date, the mechanisms causing inflammation
399 remain unclear and medical intervention is limited to the treatment of symptoms. Interestingly, Sia related genes,
400 such as the sialyltransferase ST6Gal1, Siglec-6 and sialic acid acetylesterase (SIAE) are reported to be differentially
401 regulated in placentae of preeclamptic women, providing a first clue that aberrant sialylation might be involved in
402 this pathology (62,63). Further studies are needed to fully evaluate the molecular details by which sialylation
403 might be involved in the pathogenesis of pregnancy complications and if the absence of specific sialoglycans could
404 serve as a potential diagnostic marker.

405 In conclusion, the constitutive *Cmas* mouse model presented here and its available conditional variants are
406 valuable tools to specifically investigate the impact of sialylation on the regulation of the complement system, not
407 only during pregnancy but also in immunologically challenging situations, e.g. after organ transplantations.

409 **METHODS**410 **Mice**

411 To inactivate the *Cmas* gene, exon 4 encoding for the active site of the protein was deleted using the frt/loxP
 412 system as described (9). The neomycin-cassette was deleted by crossing *Cmas^{neo}* homozygous mice with the Flp-
 413 deleter strain *SJL-Tg(ACTFLPe)9205Dym/J*. Resulting *Cmas^{flaxed}* mice were bred to homozygosity and crossed with
 414 the Cre-deleter strain *C57BL/6-Tg(Zp3-cre)93Knw/J*. Upon six backcrosses with NMRI mice heterozygous *Cmas*
 415 knockout mice (*Cmas^{+/−}*) were obtained. Intercrosses of 3-6 month old *Cmas^{+/−}* animals gave rise to *Cmas^{−/−}*, *Cmas^{+/−}*
 416 and *Cmas^{+/+}* embryos, the latter two referred to as controls. Genotyping was done by PCR as depicted in Figure
 417 S1A, B. The following primers were used: BWF59 (5`AGCGCCTGTGTACCCCTTTA3`), BWB58
 418 (5`GCGAGCAGCAAGTGAGCA3`) and AMB40 (5`TCAAGTTCAGAGGCTAGTCACCCACG3`); the PCR program
 419 included three steps (98°C 30sec, 66°C 30sec, 72°C 30sec) and 30 cycles. Animals were obtained from and hosted
 420 in the animal facility of the Hannover Medical School under specific pathogen-free conditions. All animal
 421 experiments were carried out in compliance with German law for protection of animals and were approved by the
 422 local authorities (TV 33.12–42502-04-16/2346).

423 **Histology and quantification of IUGR**

424 Female mice of heterozygous *Cmas^{+/−}* matings were checked daily in the early morning for vaginal plug. The time
 425 point of plug discovery was considered as day 0.5 after conception. On day 6.5, 7.5 and 8.5 of gestation, pregnant
 426 mice were sacrificed, and the uteri were dissected and fixed in 4% paraformaldehyde in PBS o/n at 4°C. After
 427 fixation, the uteri were dehydrated in a graded ethanol series and embedded in paraffin. For histological analyses,
 428 paraffin embedded uteri were sectioned in 3 µm slices using a microtome, rehydrated and stained with
 429 hematoxylin and eosin. Slices were analysed by a Zeiss ObserverZ1 microscope equipped with a Zeiss AxioCam
 430 MRc camera. To quantify intrauterine growth restriction, the sum of the areas of amniotic cavity, exocoelomic
 431 cavity, ectoplacental cavity and embryo proper as depicted in Figure S3 were measured using Zeiss ZEN software.
 432 Statistical analyses were performed in GraphPad Prism software where P < 0.05 was considered significant.

433 **Lectin assays on uterus sections**

434 For detection of α2,3-linked sialic acid rehydrated tissue slices were probed with *Maackia amurensis* agglutinin,
 435 1:800 (MAA, DIG Glycan Differentiation Kit, Roche) at 4°C o/n with subsequent incubation with peroxidase
 436 coupled anti-DIG Fab fragments, 1:1000 (Roche). Signals were enhanced by biotin tyramide, 2,5 µg/ml (Iris
 437 Biotech) amplification for 10 minutes at room temperature and detected by Streptavidin-Cy3, 1:2000 (Rockland).
 438 For detection of α2,6-linked sialic acid rehydrated tissue slices were probed with biotinylated *Sambucus nigra*
 439 agglutinin, 1:250 (SNA, Vector) at 4°C o/n with subsequent detection by Streptavidin-Cy3, 1:500 (Rockland).
 440 Control slides were treated with *Arthrobacter ureafaciens* neuraminidase (EY Laboratories) at room temperature
 441 o/n prior to MAA incubation. For simultaneous detection of free galactose residues, Alexa Fluor® 647 conjugated
 442 *Arachis hypogaea* agglutinin (PNA, Sigma-Aldrich) was added during incubation with Streptavidin-Cy3. Decidual NK
 443 cells were detected by biotinylated *Dolichos biflorus* agglutinin (DBA), 1:2000 (Vector) and subsequently stained
 444 with streptavidin-HRP, 1:500 (Vector). DBA positive cells were detected by 3,3'-Diaminobenzidine (DAB, Dako)
 445 reaction, subsequently counterstained with hematoxylin and analysed in the aforementioned microscope setup.

446 **Immunohistochemistry and indirect immunofluorescence analyses**

447 Tissues were paraffin fixed and embedded according to H&E staining. For immunohistochemistry (IHC) and
 448 immunofluorescence analyses, antigen retrieval (Dako) was performed after rehydration. Slices were then
 449 blocked with 1% BSA in PBS and incubated with the respective antibody in blocking solution. The following
 450 dilutions for primary antibodies were applied: Cytokeratin-8, 1:20.00 (TROMA-I, DSHB, AB 531826); Collagen-IV,
 451 1:200 (Millipore, AB756P); Laminin, 1:30 (Sigma, L9393); Gr-1, 1:50 (BD Biosciences, RB6-8C5); F4/80, 1:50 (AbD
 452 Serotec, Cl:A3-1); anti-Ly6G, 1:100.000 (BioXCell, 1A8) ; C3, 1:20.000 (Cappel, MP Biomedicals, 55463); C1q 1:50

453 (Biorbyt, orb155963), C4d 1:50 (Hycult Biotech, HP8033); Properdin 1:2000 (Complement Technologies, A139); C9
454 1:10.000 (Paul B. Morgan, University Hospital of Wales, Cardiff University, Heath Park, Cardiff, CF14 4XN, UK),
455 Cebpb, 1:20 (Santa Cruz, H-7). Cebpb antibody was pre-incubated with biotinylated anti-mouse IgG Fab fragments
456 prior to use (ARK kit, Dako, K3954) according to the manufacturer's guidelines. Secondary antibodies: anti-rabbit
457 IgG-Cy3, 1:500 (Sigma, C2306); anti-rabbit IgG- 1:500 (Sigma, A0545); anti-goat IgG, 1:500 (Santa Cruz, SC-2020).
458 Biotinylation was detected using strepavidin-HRP, 1:500 (Dako, P0397) and the signal was amplified by biotin
459 tyramide, 2,5 µg/ml (Iris Biotech) treatment for 10 minutes at room temperature. Streptavidin-Cy3, 1:500
460 (Rockland, S000-04) served as detection system). For detection of Gr-1 a biotinylated anti-rat antibody (1:500,
461 Boehringer, 1348779) was used, followed by strepavidin-HRP, 1:500 (Dako, P0397). Cytokeratin-8 and Ly6G were
462 detected using the ImmPRESS™ HRP anti-rat IgG (Vector, MP-7444) conjugate. All HRP-conjugated reagents were
463 detected by 3,3'-Diaminobenzidine (DAB) reaction, subsequently counterstained with hematoxylin and analysed
464 in the aforementioned microscope setup.

465 **In situ hybridisation experiments**

466 In situ hybridizations were performed on 10 µm sections. Riboprobes were synthesised by T3 or T7 polymerases
467 using DIG-labelled UTP (Roche). Specific hybridisation was detected by incubation with anti-DIG alkaline
468 phosphatase (Roche) and subsequent staining with BCIP/NBT.

469 **Quantification of decidual leukocyte populations**

470 Identification of leukocytes was accomplished by IHC of described marker proteins, i.e. Gr-1/Ly6G (neutrophils),
471 DBA (decidual NK cells) or F4/80 (macrophages). Gr-1/Ly6G positive cells located in the maternal decidua were
472 counted, whereby positive cells in the maternal vasculature were excluded. Also F4/80 positive cells were
473 quantified in the entire maternal decidua. DBA positive cells were quantified in the decidua basalis. In all of the
474 mentioned leukocyte quantifications, also the total area of the decidua was measured and the ratio of positive
475 leukocytes per mm² (for Gr-1, Ly6G and F4/80) or µm²/10⁵ (for DBA) was calculated. For comparing decidual
476 leukocytes of control versus *Cmas*^{+/−} implants a Student's t-test was applied.

477 **Depletion of neutrophils from maternal blood**

478 Heterozygous *Cmas*^{+/−} mice were mated as described and 500 µg anti-Ly6G (1A8, BioXCell) or isotype control
479 antibody (2A3, BioXCell) diluted in 100 µl PBS were intraperitoneally injected into pregnant mice at day E4.5. The
480 uteri of Ly6G treated mice were removed at E8.5 and the uterus of the isotype control treated mouse was
481 removed at E9.5. To verify the successful depletion of maternal neutrophils, blood from Ly6G or from untreated
482 mice was analysed by FACS in a FACScalibur machine (Beckton & Dickinson) and raw data were analysed using
483 FlowJo (TreeStar). Blood was obtained from the abdominal aorta with a heparinised syringe after cervical
484 dislocation and treated with red blood cell lysis buffer for 10 minutes at room temperature. For the FACS analyses
485 0,2 mg/ml anti-Ly6G (1A8, BioXCell) or 0,2 mg/ml isotype control rat IgG2a (2A3, BioXCell) was used as primary
486 antibody and anti-rat IgG-Cy3, 1:200 (AP189C, EMD Millipore) as secondary antibody. Cells were gated for
487 lymphocytes, monocytes and granulocytes using the forward scatter, before subsequent analysis of Ly6G positive
488 cells.

489 **Decomplementation of pregnant mice**

490 Three individual pregnant *Cmas*^{+/−} mice were intraperitoneally injected at E4.5 and E6.5 two times at these days at
491 10 am and 2 pm with either 5 U of cobra venom factor (CVF) (Quidel) in 100 µl PBS or PBS only for each injection.
492 They were killed at day 8.5 of pregnancy and *Cmas*^{+/−} and control littermates were analysed. Depletion of C3 in the
493 serum of CVF treated animals was confirmed by western blot: 0.25 µl serum was separated by 12% SDS-PAGE
494 under reducing conditions, transferred to PVDF membrane and incubated with the primary antibodies goat anti-
495 C3, 1:5.000 (Cappel, MP Biomedicals) or goat anti-albumin, 1:5.000 (ab19194, Abcam) for loading control. After

496 incubation with anti-goat HRP-conjugated secondary antibody, 1:15.000 (sc-2020, Santa Cruz) detection was
497 performed with enhanced chemoluminescence.

498 **Statistics**

499 Comparisons of fetal size (Figure 2B, Figure 4C), Gr-1 positive cells (Figure 3A), DBA positive cells (Figure 3A) and
500 F4/80 positive cells (Figure 3A, Figure S7) were analysed by two-tailed unpaired *t* test. Statistical analysis of
501 quantifications of Ly6G positive cells (Figure 6A), fetal size (Figure 6D) and Reichert's membrane thickness (Figure
502 6C) after treatment with CVF or PBS were analysed by one-way ANOVA, followed by Newman-Keuls post-test. All
503 analyses were performed using GraphPad Prism software and P < 0,05 was considered significant.

504 **Study approval**

505 All animal experiments were approved by the "Niedersaechsisches Landesamt fuer Verbraucherschutz und
506 Lebensmittelsicherheit (LAVES)", Postfach 3949, 26029 Oldenburg, Germany, AZ 33.12-42502-04-16/2346 and
507 from the „Institut fuer Versuchstierkunde und Zentrales Tierlaboratorium“, Hannover Medical School, Carl-
508 Neuberg-Str. 1, 30625 Hannover, Germany, Head Prof. Andre Bleich.

509 **Author contributions**

510 Conceptualisation, R.G.S., A.M.K. and B.W.; Methodology, M.A., A.M.K., A.K., S.T. and B.W.; Validation, M.A. and
511 B.W.; Formal analysis, M.A. and B.W.; Investigation, M.A., I.A., K.F.S. and U.B.P.; Generation of *Cmas* mutant mice,
512 B.W.; Resources, A.K., R.G.S., S.T., A.M.K. and B.W.; Writing-Original Draft, M.A., A.M.K. and B.W.; Visualisation,
513 M.A. and B.W.; Supervision, R.G.S., A.M.K. and B.W., Funding Acquisition, R.G.S., A.M.K. and B.W.

514

515 **Acknowledgements**

516 We thank Mania Ackermann for help with the FACS analyses, Carina Weiss for support regarding in situ
517 hybridisations and Adrian Erlebacher and Susan Fisher for critical and helpful discussion of the data. Also we
518 would like to thank Paul B. Morgan (Cardiff University) for kindly providing anti-C9 antibody. Anja Münster-Kühnel
519 and Birgit Weinhold were supported by grants from the Deutsche Forschungsgemeinschaft (DFG, MU 1849/2-1
520 and WE 5585/1-1).

References

1. Moremen KW, Tiemeyer M, Nairn AV. Vertebrate protein glycosylation: diversity, synthesis and function. *Nat Rev Mol Cell Biol.* 2012;13(7):448-462.
2. Fujitani N, Furukawa J, Araki K, Fujioka T, Takegawa Y, Piao J, Nishioka T, Tamura T, Nikaido T, Ito M *et al.* Total cellular glycomics allows characterizing cells and streamlining the discovery process for cellular biomarkers. *Proc Natl Acad Sci U S A.* 2013;110(6):2105-2110.
3. Cohen M, Varki A. The sialome--far more than the sum of its parts. *OMICS.* 2010;14(4):455-464.
4. Bhide GP, Colley KJ. Sialylation of N-glycans: mechanism, cellular compartmentalization and function. *Histochem Cell Biol.* 2017;147(2):149-174.
5. Blaum BS, Hannan JP, Herbert AP, Kavanagh D, Uhrin D, Stehle T. Structural basis for sialic acid-mediated self-recognition by complement factor H. *Nat Chem Biol.* 2015;11(1):77-82.
6. Crocker PR, Paulson JC, Varki A. Siglecs and their roles in the immune system. *Nat Rev Immunol.* 2007;7(4):255-266.
7. Varki A, Gagneux P. Multifarious roles of sialic acids in immunity. *Ann N Y Acad Sci.* 2012;1253:16-36.
8. Kean EL, Münster-Kühnel AK, Gerardy-Schahn R. CMP-sialic acid synthetase of the nucleus. *Biochim Biophys Acta.* 2004;1673(1-2):56-65.
9. Abeln M, Borst KM, Cajic S, Thiesler H, Kats E, Albers I, Kuhn M, Kaever V, Rapp E, Münster-Kühnel A *et al.* Sialylation Is Dispensable for Early Murine Embryonic Development in Vitro. *Chembiochem.* 2017;18(13):1305-1316.
10. Schwarzkopf M, Knobeloch KP, Rohde E, Hinderlich S, Wiechens N, Lucka L, Horak I, Reutter W, Horstkorte R. Sialylation is essential for early development in mice. *Proc Natl Acad Sci U S A.* 2002;99(8):5267-5270.
11. Prabhudas M, Bonney E, Caron K, Dey S, Erlebacher A, Fazleabas A, Fisher S, Golos T, Matzuk M, McCune JM *et al.* Immune mechanisms at the maternal-fetal interface: perspectives and challenges. *Nat Immunol.* 2015;16(4):328-334.
12. Marikawa Y, Alarcon VB. Establishment of trophectoderm and inner cell mass lineages in the mouse embryo. *Mol Reprod Dev.* 2009;76(11):1019-1032.
13. Bielinska M, Narita N, Wilson DB. Distinct roles for visceral endoderm during embryonic mouse development. *Int J Dev Biol.* 1999;43(3):183-205.
14. Schröde N, Xenopoulos P, Piliszek A, Frankenberg S, Plusa B, Hadjantonakis AK. Anatomy of a blastocyst: cell behaviors driving cell fate choice and morphogenesis in the early mouse embryo. *Genesis.* 2013;51(4):219-233.
15. Watson ED, Cross JC. Development of structures and transport functions in the mouse placenta. *Physiology (Bethesda).* 2005;20:180-193.

16. Rai A, Cross JC. Development of the hemochorial maternal vascular spaces in the placenta through endothelial and vasculogenic mimicry. *Dev Biol.* 2014;387(2):131-141.
17. Apps R, Murphy SP, Fernando R, Gardner L, Ahad T, Moffett A. Human leucocyte antigen (HLA) expression of primary trophoblast cells and placental cell lines, determined using single antigen beads to characterize allotype specificities of anti-HLA antibodies. *Immunology.* 2009;127(1):26-39.
18. Hunt JS, Fishback JL, Andrews GK, Wood GW. Expression of class I HLA genes by trophoblast cells. Analysis by *in situ* hybridization. *J Immunol.* 1988;140(4):1293-1299.
19. Madeja Z, Yadi H, Apps R, Boulenouar S, Roper SJ, Gardner L, Moffett A, Colucci F, Hemberger M. Paternal MHC expression on mouse trophoblast affects uterine vascularization and fetal growth. *Proc Natl Acad Sci U S A.* 2011;108(10):4012-4017.
20. Holmes CH, Simpson KL, Okada H, Okada N, Wainwright SD, Purcell DF, Houlihan JM. Complement regulatory proteins at the feto-maternal interface during human placental development: distribution of CD59 by comparison with membrane cofactor protein (CD46) and decay accelerating factor (CD55). *Eur J Immunol.* 1992;22(6):1579-1585.
21. Xu C, Mao D, Holers VM, Palanca B, Cheng AM, Molina H. A critical role for murine complement regulator Crry in fetomaternal tolerance. *Science.* 2000;287(5452):498-501.
22. Nancy P, Tagliani E, Tay CS, Asp P, Levy DE, Erlebacher A. Chemokine gene silencing in decidual stromal cells limits T cell access to the maternal-fetal interface. *Science.* 2012;336(6086):1317-1321.
23. Zhao H, Kalish F, Schulz S, Yang Y, Wong RJ, Stevenson DK. Unique roles of infiltrating myeloid cells in the murine uterus during early to midpregnancy. *J Immunol.* 2015;194(8):3713-3722.
24. Girardi G, Berman J, Redecha P, Spruce L, Thurman JM, Kraus D, Hollmann TJ, Casali P, Carroll MC, Wetsel RA et al. Complement C5a receptors and neutrophils mediate fetal injury in the antiphospholipid syndrome. *J Clin Invest.* 2003;112(11):1644-1654.
25. Jeyabalan A. Epidemiology of preeclampsia: impact of obesity. *Nutr Rev.* 2013;71 Suppl 1:S18-S25.
26. Srinivas SK, Edlow AG, Neff PM, Sammel MD, Andrela CM, Elovitz MA. Rethinking IUGR in preeclampsia: dependent or independent of maternal hypertension? *J Perinatol.* 2009;29(10):680-684.
27. Novogrodsky A, Lotan R, Ravid A, Sharon N. Peanut agglutinin, a new mitogen that binds to galactosyl sites exposed after neuraminidase treatment. *J Immunol.* 1975;115(5):1243-1248.
28. Simmons DG, Cross JC. Determinants of trophoblast lineage and cell subtype specification in the mouse placenta. *Dev Biol.* 2005;284(1):12-24.
29. Tamai Y, Ishikawa T, Bosl MR, Mori M, Nozaki M, Baribault H, Oshima RG, Taketo MM. Cytokeratins 8 and 19 in the mouse placental development. *J Cell Biol.* 2000;151(3):563-572.
30. Jollie WP. Changes in the fine structure of the parietal yolk sac of the rat placenta with increasing gestational age. *Am J Anat.* 1968;122(3):513-531.

31. Sheng G, Foley AC. Diversification and conservation of the extraembryonic tissues in mediating nutrient uptake during amniote development. *Ann N Y Acad Sci.* 2012;1271:97-103.
32. Croy BA, Chantakru S, Esadeg S, Ashkar AA, Wei Q. Decidual natural killer cells: key regulators of placental development (a review). *J Reprod Immunol.* 2002;57(1-2):151-168.
33. Zhang JH, Yamada AT, Croy BA. DBA-lectin reactivity defines natural killer cells that have homed to mouse decidua. *Placenta.* 2009;30(11):968-973.
34. Daley JM, Thomay AA, Connolly MD, Reichner JS, Albina JE. Use of Ly6G-specific monoclonal antibody to deplete neutrophils in mice. *J Leukoc Biol.* 2008;83(1):64-70.
35. Lynch AM, Salmon JE. Dysregulated complement activation as a common pathway of injury in preeclampsia and other pregnancy complications. *Placenta.* 2010;31(7):561-567.
36. van den Berg CW, Aerts PC, Van Dijk H. In vivo anti-complementary activities of the cobra venom factors from *Naja naja* and *Naja haje*. *J Immunol Methods.* 1991;136(2):287-294.
37. Begay V, Smink J, Leutz A. Essential requirement of CCAAT/enhancer binding proteins in embryogenesis. *Mol Cell Biol.* 2004;24(22):9744-9751.
38. Simmons DG, Natale DR, Begay V, Hughes M, Leutz A, Cross JC. Early patterning of the chorion leads to the trilaminar trophoblast cell structure in the placental labyrinth. *Development.* 2008;135(12):2083-2091.
39. Murata K, Baldwin WM, III. Mechanisms of complement activation, C4d deposition, and their contribution to the pathogenesis of antibody-mediated rejection. *Transplant Rev (Orlando).* 2009;23(3):139-150.
40. Hourcade DE. The role of properdin in the assembly of the alternative pathway C3 convertases of complement. *J Biol Chem.* 2006;281(4):2128-2132.
41. Maltepe E, Fisher SJ. Placenta: the forgotten organ. *Annu Rev Cell Dev Biol.* 2015;31:523-552.
42. Nadeau-Vallee M, Obari D, Palacios J, Brien ME, Duval C, Chemtob S, Girard S. Sterile inflammation and pregnancy complications: a review. *Reproduction.* 2016;152(6):R277-R292.
43. Varki A. Glycan-based interactions involving vertebrate sialic-acid-recognizing proteins. *Nature.* 2007;446(7139):1023-1029.
44. Chen Q, Pang PC, Cohen ME, Longtine MS, Schust DJ, Haslam SM, Blois SM, Dell A, Clark GF. Evidence for Differential Glycosylation of Trophoblast Cell Types. *Mol Cell Proteomics.* 2016;15(6):1857-1866.
45. Bevilacqua E, Hoshida MS, Amarante-Paffaro A, Albieri-Borges A, Zago GS. Trophoblast phagocytic program: roles in different placental systems. *Int J Dev Biol.* 2010;54(2-3):495-505.
46. Bedzhov I, Graham SJ, Leung CY, Zernicka-Goetz M. Developmental plasticity, cell fate specification and morphogenesis in the early mouse embryo. *Philos Trans R Soc Lond B Biol Sci.* 2014;369(1657).
47. Macauley MS, Crocker PR, Paulson JC. Siglec-mediated regulation of immune cell function in disease. *Nat Rev Immunol.* 2014;14(10):653-666.

48. Lock K, Zhang J, Lu J, Lee SH, Crocker PR. Expression of CD33-related siglecs on human mononuclear phagocytes, monocyte-derived dendritic cells and plasmacytoid dendritic cells. *Immunobiology*. 2004;209(1-2):199-207.
49. McMillan SJ, Sharma RS, McKenzie EJ, Richards HE, Zhang J, Prescott A, Crocker PR. Siglec-E is a negative regulator of acute pulmonary neutrophil inflammation and suppresses CD11b beta2-integrin-dependent signaling. *Blood*. 2013;121(11):2084-2094.
50. Chang YC, Olson J, Beasley FC, Tung C, Zhang J, Crocker PR, Varki A, Nizet V. Group B Streptococcus engages an inhibitory Siglec through sialic acid mimicry to blunt innate immune and inflammatory responses in vivo. *PLoS Pathog*. 2014;10(1):e1003846.
51. Giaglis S, Stoikou M, Grimolizzi F, Subramanian BY, van Breda SV, Hoesli I, Lapaire O, Hasler P, Than NG, Hahn S. Neutrophil migration into the placenta: Good, bad or deadly? *Cell Adh Migr*. 2016;10(1-2):208-225.
52. McMillan SJ, Sharma RS, Richards HE, Hegde V, Crocker PR. Siglec-E promotes beta2-integrin-dependent NADPH oxidase activation to suppress neutrophil recruitment to the lung. *J Biol Chem*. 2014;289(29):20370-20376.
53. Goldman JN, Bangalore S, Goldman MB. Activation of murine complement by cobra venom factor in the presence of EDTA. *J Immunol*. 1979;123(5):2421-2427.
54. Chenoweth DE, Goodman MG, Weigle WO. Demonstration of a specific receptor for human C5a anaphylatoxin on murine macrophages. *J Exp Med*. 1982;156(1):68-78.
55. Quell KM, Karsten CM, Kordowski A, Almeida LN, Briukhovetska D, Wiese AV, Sun J, Ender F, Antoniou K, Schroder T et al. Monitoring C3aR Expression Using a Floxed tdTomato-C3aR Reporter Knock-in Mouse. *J Immunol*. 2017;199(2):688-706.
56. Mao D, Wu X, Deppong C, Friend LD, Dolecki G, Nelson DM, Molina H. Negligible role of antibodies and C5 in pregnancy loss associated exclusively with C3-dependent mechanisms through complement alternative pathway. *Immunity*. 2003;19(6):813-822.
57. Ferreira VP, Pangburn MK, Cortes C. Complement control protein factor H: the good, the bad, and the inadequate. *Mol Immunol*. 2010;47(13):2187-2197.
58. Hyvarinen S, Meri S, Jokiranta TS. Disturbed sialic acid recognition on endothelial cells and platelets in complement attack causes atypical hemolytic uremic syndrome. *Blood*. 2016;127(22):2701-2710.
59. Ricklin D, Reis ES, Lambris JD. Complement in disease: a defence system turning offensive. *Nat Rev Nephrol*. 2016;12(7):383-401.
60. Sibai B, Dekker G, Kupferminc M. Pre-eclampsia. *Lancet*. 2005;365(9461):785-799.
61. Wang W, Irani RA, Zhang Y, Ramin SM, Blackwell SC, Tao L, Kellems RE, Xia Y. Autoantibody-mediated complement C3a receptor activation contributes to the pathogenesis of preeclampsia. *Hypertension*. 2012;60(3):712-721.
62. Tsai S, Hardison NE, James AH, Motsinger-Reif AA, Bischoff SR, Thames BH, Piedrahita JA. Transcriptional profiling of human placentas from pregnancies complicated by preeclampsia reveals disregulation of sialic acid acetyltransferase and immune signalling pathways. *Placenta*. 2011;32(2):175-182.

63. Winn VD, Gormley M, Paquet AC, Kjaer-Sorensen K, Kramer A, Rumer KK, Haimov-Kochman R, Yeh RF, Overgaard MT, Varki A *et al.* Severe preeclampsia-related changes in gene expression at the maternal-fetal interface include sialic acid-binding immunoglobulin-like lectin-6 and pappalysin-2. *Endocrinology*. 2009;150(1):452-462.

Figure 1. *Cmas*^{-/-} embryos lack sialylation. **(A)** Lectin binding epitopes for *Maackia amurensis* agglutinin (MAA) detecting terminal α2,3 linked sialic acid and for peanut agglutinin (PNA) detecting terminal galactose. **(B)** Sagittal paraffin sections of uteri with E6.5 and E8.5 implants were co-stained with the lectins MAA (red) and PNA (green). Insets show trophoblast giant cells lining the fetal-maternal interface. The area of the ecotrophoblastic cone (EPC) is indicated by brackets. MAA positive cells in *Cmas*^{-/-} (inset, magnified) are maternal leukocytes. Asterisks indicate Reichert's membrane; arrows mark the apical side of ectodermal epithelia and arrowheads indicate mesenchymal cells. MAA specificity was confirmed by neuraminidase treatment of sagittal paraffin sections prior to lectin staining. Neuraminidase releases sialic acid from glycans and thereby depletes MAA binding epitopes. Simultaneously, removal of Sia exposes underlying galactose to PNA binding. Scale bar in the insets: 50 μm. Nuclei were stained with DAPI and are shown in white. Representative images from n=3 (E6.5 control and *Cmas*^{-/-}, E8.5 *Cmas*^{-/-}) and n=5 (E8.5 control) embryos within uterus.

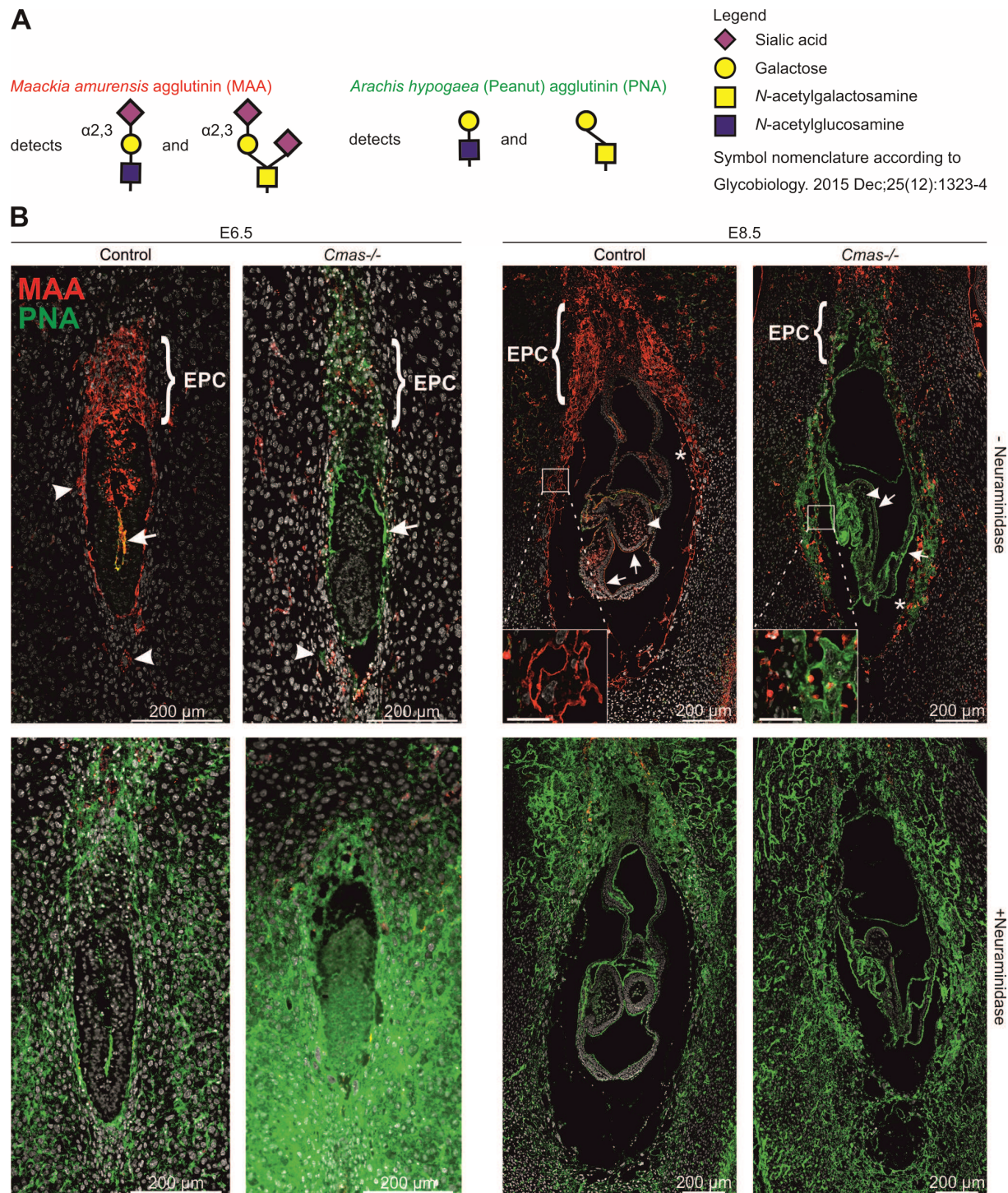


Figure 2. *Cmas*^{-/-} mice exhibit intrauterine growth restriction and extraembryonic developmental deficits. (A) Hematoxylin and eosin stained sagittal paraffin sections of uteri at E6.5, E7.5 and E8.5. Insets show mesenchymal mesoderm cells migrating from posterior to anterior. Proamniotic cavity (PC); visceral endoderm (VE); embryonic ectoderm (EC); mesoderm (ME); heart (H); somite (S). Scale bars in the insets: 12.5 µm. Representative images of at least 3 embryos within the uterus for each genotype and time point. (B) Mean fetal size as measured by the sum of the areas of amniotic cavity, exocoelomic cavity, ectoplacental cavity and embryo proper in ($\mu\text{m}^2/10^5$), for schematic overview of measured areas see Figure S5. E6.5 (control n=4, *Cmas*^{-/-} n=5), E7.5 (control n=4, *Cmas*^{-/-} n=4), E8.5 (control n=6, *Cmas*^{-/-} n=7). Error bars indicate SD. Statistical analyses were performed by Student's t-test. (*P < 0.05). (C) Immunohistochemical detection of Cytokeratin-8 as marker for trophoblast cells on sagittal paraffin sections of E8.5 uteri. Trophoblast giant cells (TGC) and the chorionic plate (CP) are indicated by arrows, internal trophoblasts of the EPC by arrowheads. The border of the ectoplacental cone (EPC) is marked by dotted lines. Representative images of n=3 embryos for each genotype. (D) Collagen IV and Laminin indirect immunofluorescence staining on sagittal paraffin sections of uteri at E8.5 to visualise Reichert's membrane (arrow) and parietal endoderm (arrowheads). Nuclei stained with DAPI are shown in white. Representative images of n=3 embryos for each genotype.

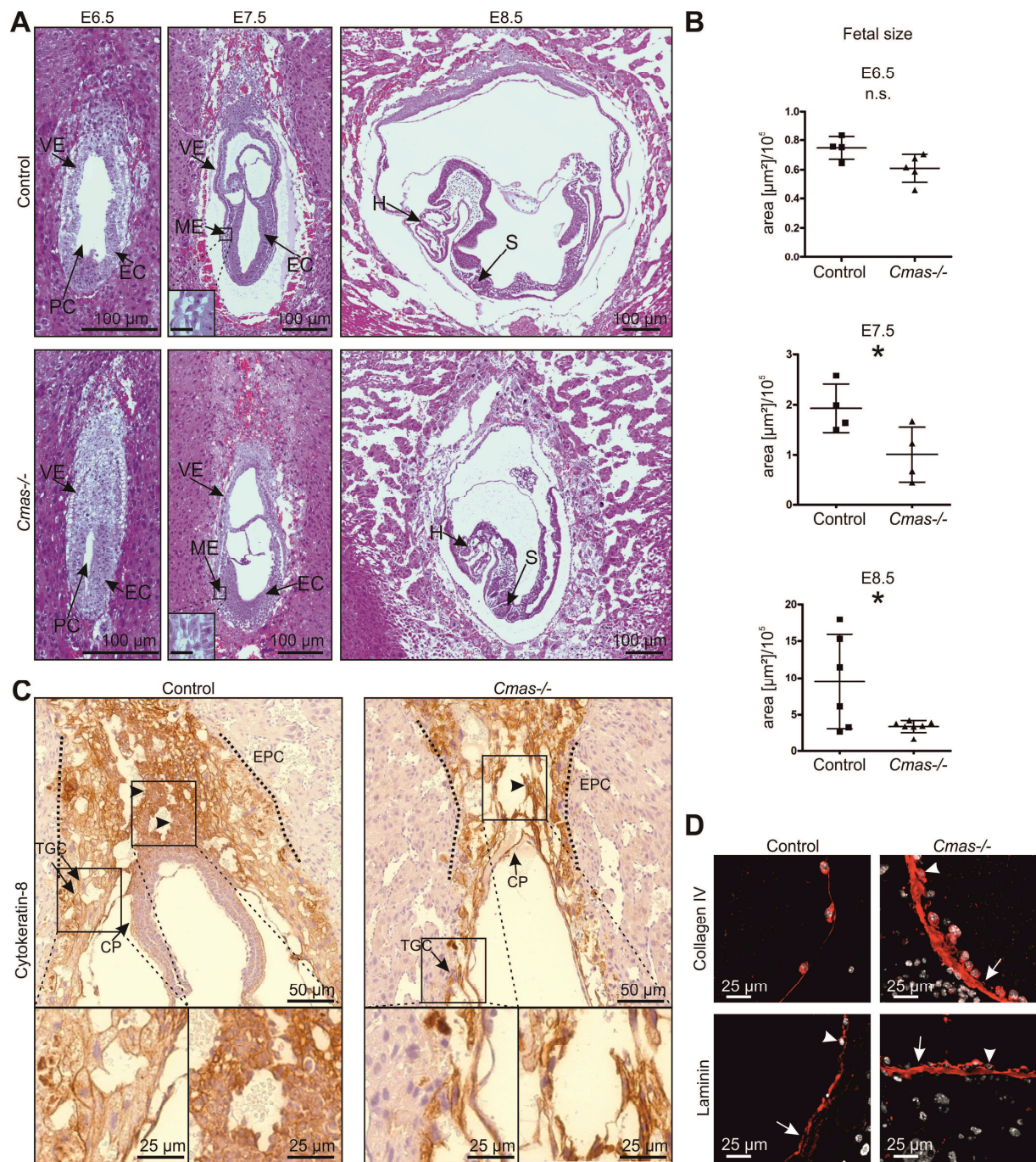


Figure 3. Infiltration of the fetal-maternal interface of *Cmas*^{-/-} animals by maternal neutrophils. (A) Gr-1 (neutrophils) immunohistochemical staining and quantification of Gr-1-positive cells surrounding fetal tissues of sagittal paraffin sections of uteri at E6.5 to E8.5. Insets show Gr-1 positive cells at the ectoplacental cone and in the vicinity of fetal trophoblasts at the antimesometrial pole. E6.5 (control n=4, *Cmas*^{-/-} n=5), E7.5 (control n=4, *Cmas*^{-/-} n=4) and E8.5 (control n=5, *Cmas*^{-/-} n=5). Error bars indicate SD. Scale bars in the insets: 12.5 μ m. (B) DBA lectin (decidual NK cells) immunohistochemical staining and quantification of sagittal paraffin sections of uteri at E6.5 to E8.5. Mean number of DBA lectin positive cells in the decidua basalis. E6.5 (control n=4, *Cmas*^{-/-} n=5), E7.5 (control n=8, *Cmas*^{-/-} n=5), E8.5 (control n=5, *Cmas*^{-/-} n=3). Error bars indicate SD. Staining of visceral endoderm was only observed in control implants. (C) F4/80 (macrophages) immunohistochemical staining and quantification of sagittal paraffin sections of uteri from E6.5 to E8.5. Statistical analysis of the number of F4/80 positive cells surrounding fetal tissues. E6.5 (control n=4, *Cmas*^{-/-} n=4), E7.5 (control n=6, *Cmas*^{-/-} n=5), E8.5 (control n=4, *Cmas*^{-/-} n=5). Scale bars in the insets: 25 μ m. Error bars indicate SD. All statistical analyses were performed by Student's t-test **P < 0.01; ***P < 0.001.

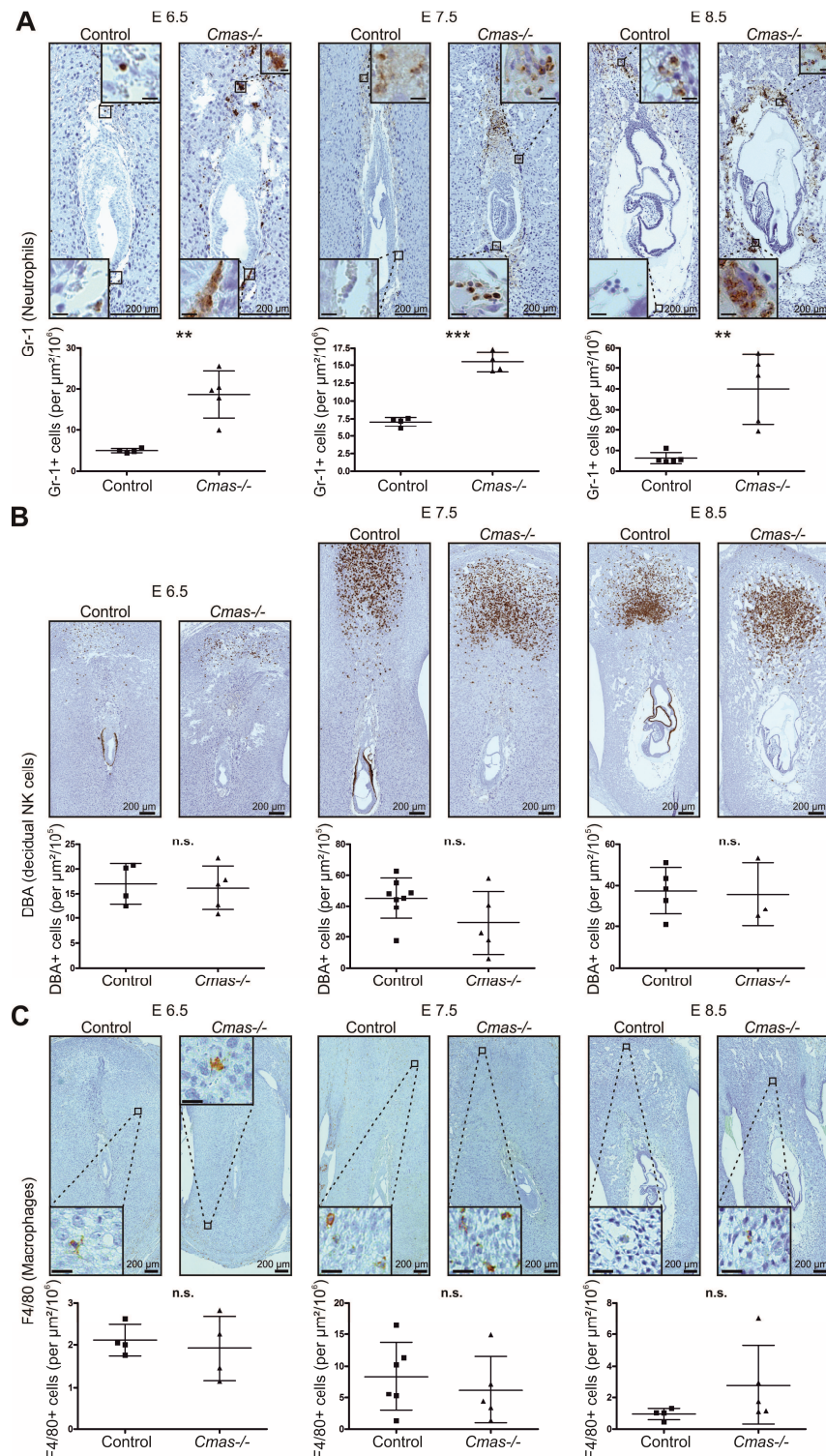


Figure 4. Depletion of maternal neutrophils does not rescue the *Cmas*^{-/-} phenotype. (A) Neutrophils were depleted by intraperitoneal injection of 500 µg anti-Ly6G antibody (1A8, BioXCell) into pregnant mice at E4.5. Ly6G FACS analysis of whole blood from untreated and anti-Ly6G injected pregnant mice at day E8.5. (B) Ly6G (neutrophils) immunohistochemical staining of sagittal paraffin sections of embryos within the uterus. Pregnant females were either treated with the isotype antibody (2A3, BioXCell) as a negative control or with anti-Ly6G for neutrophil depletion. Representative images of control (n=6) and *Cmas*^{-/-} (n=4) embryos. (C) Mean fetal size of control and *Cmas*^{-/-} embryos from anti-Ly6G treated mother mice as measured by the sum of the areas of amniotic cavity, exocoelomic cavity, ectoplacental cavity and embryo proper in ($\mu\text{m}^2/10^5$) (control n=6, *Cmas*^{-/-} n=4). Schematic overview of measured areas, see Figure S5. Error bars indicate SD. Statistical analyses were performed by Student's t-test. (**P < 0.01). (D) Immunohistochemical detection of Cytokeratin-8 to visualise trophoblast cells on sagittal paraffin sections of E8.5 uteri from Ly6G treated mother mice. Representative images of control (n=6) and *Cmas*^{-/-} (n=4) embryos. (E) Collagen IV indirect immunofluorescence staining on sagittal paraffin sections of uteri at E8.5 from Ly6G treated mother mice to visualise Reichert's membrane (arrow) and parietal endoderm (arrowheads). Representative images of control (n=6) and *Cmas*^{-/-} (n=4) embryos. Nuclei stained with DAPI are shown in white.

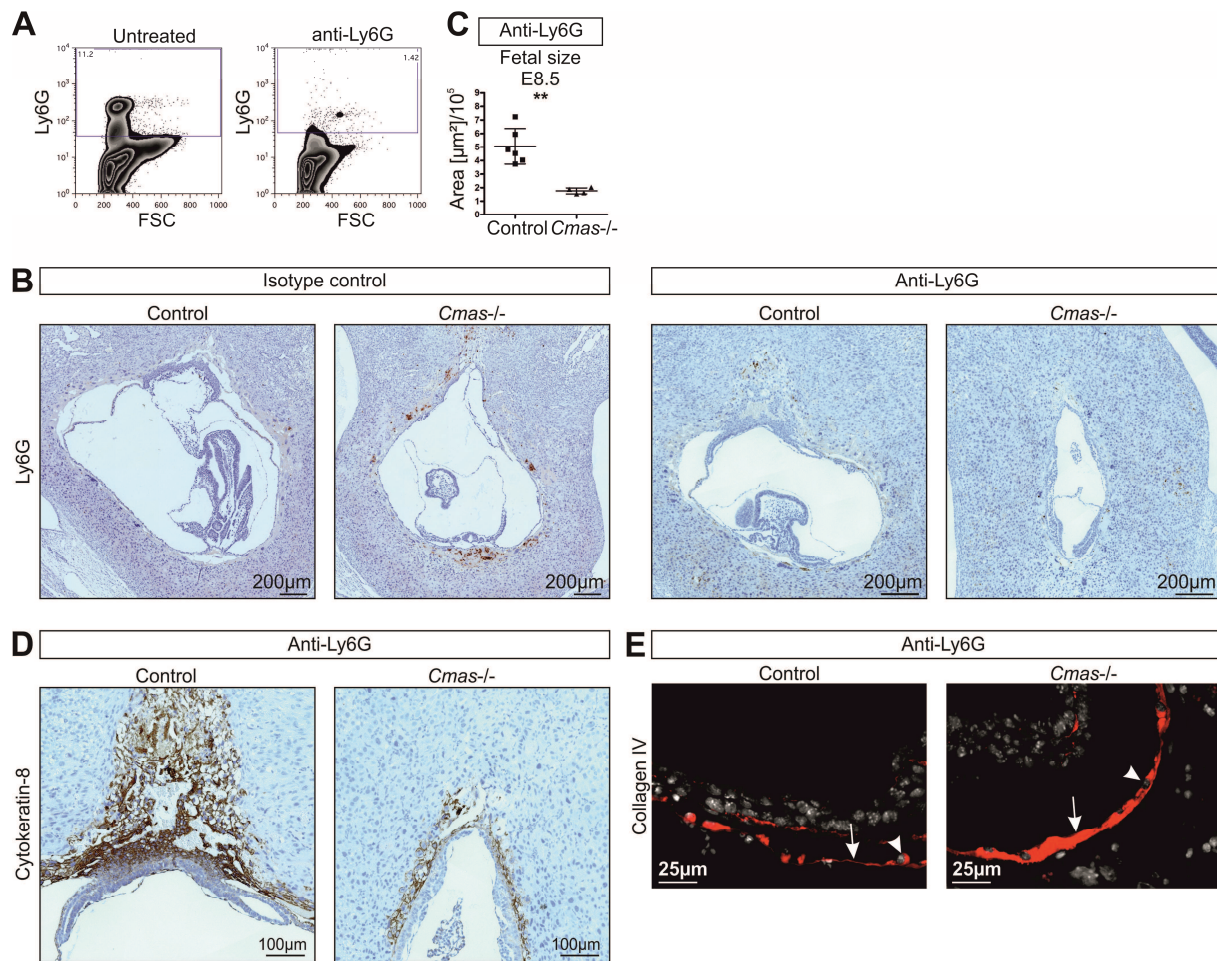


Figure 5. *Cmas*^{-/-} trophoblast cells exhibit increased deposition of complement component 3 (C3). (A) C3 immunohistochemical staining of sagittal paraffin sections of uteri at E8.5. Insets show TGCs. Scale bars in the insets: 25 μ m. C3 staining of visceral endoderm (arrowhead) was observed only in control embryos. Representative images of control (n=16) and *Cmas*^{-/-} (n=6) embryos within the uterus. **(B)** C3 immunohistochemical staining of sagittal paraffin sections of uteri at E8.5 from anti-Ly6g treated mother mice. Insets show TGCs without C3 staining on control tissue but extensive staining at TGC cell surface. Representative images of control (n=6) and *Cmas*^{-/-} (n=4) embryos within the uterus. Scale bars in the insets: 50 μ m.

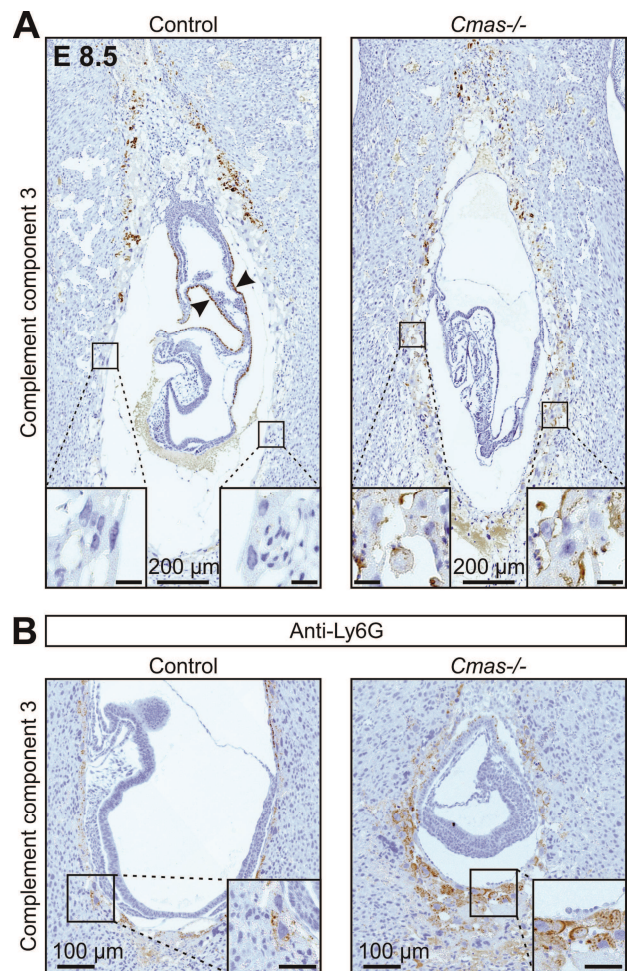


Figure 6. Cobra venom factor (CVF) decomplements the maternal serum and rescues the inflammatory phenotype of *Cmas*^{-/-} implants. (A) C3 Western Blot analysis. Serum of PBS or CVF treated pregnant mice at E8.5 was separated by SDS-PAGE and immunostained with anti-C3 antibody. C3 protein was only detectable in PBS treated mice but depleted in CVF treated pregnant mice. Anti-albumin staining as loading control. (B) C3 immunohistochemical staining of sagittal paraffin sections of E8.5 embryos within the uterus of PBS or CVF treated mice. In PBS treated mothers, C3 reactivity was restricted to the EPC in control implants, but was expanded to the entire fetal-maternal interface in *Cmas*^{-/-} embryos with strong staining at the surface of TGCs. In implants of CVF treated mothers the C3 reactivity was abolished irrespective of the genotype. Insets show fetal TGCs. (C) Ly6G immunohistochemical staining for neutrophils on sagittal paraffin sections of E8.5 uteri from PBS or CVF treated mice. Ly6G positive cells are sparsely distributed in proximity of control embryos of PBS treated mothers. In contrast, the entire fetal-maternal boundary of *Cmas*^{-/-} implants is infiltrated with Ly6G positive cells in PBS treated mice. CVF treatment does not change the phenotype of controls but reverts Ly6G staining of *Cmas*^{-/-} implants to controls. (D) Quantification of Ly6G positive cells (neutrophils) on sagittal paraffin sections of E8.5 uteri of PBS or CVF treated pregnant mice. Error bars indicate SD. Statistical analyses were performed by ANOVA with Newman-Keuls post-test (**P < 0.001). Representative images of experiments of three PBS treated pregnant mice with n=5 control and n=3 *Cmas*^{-/-} embryos, and of three CVF treated pregnant mice with n=5 control and n=4 *Cmas*^{-/-} embryos (B-D).

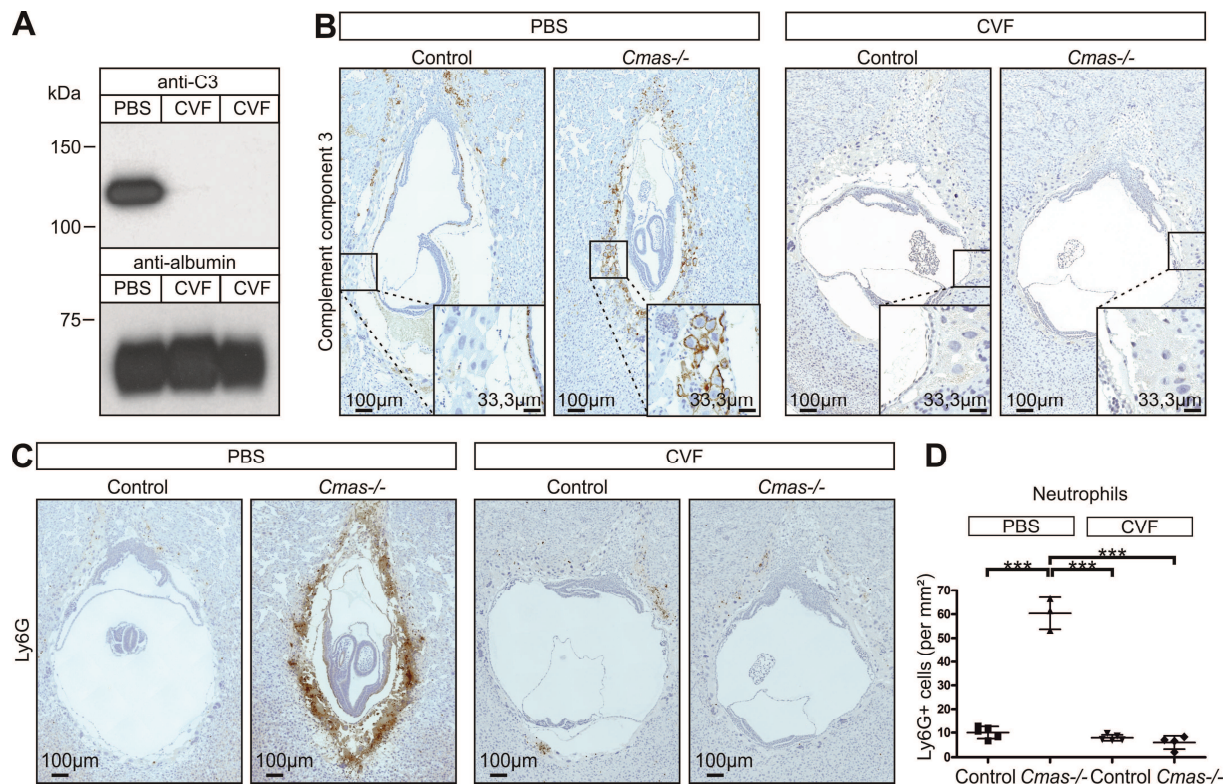


Figure 7. Maternal decomplementation rescues defects in extraembryonic tissues and growth restriction of *Cmas*^{-/-} mice. Pregnant *Cmas*^{+/-} mice were treated at E4.5 and E6.5 either with PBS (n=3) or CVF (n=3) to deplete maternal C3. E8.5 sagittal uteri paraffin sections (**A, B**). (**A**) The reduced size of the ectoplacental cone (EPC) and lack of a chorionic plate (CP) in *Cmas*^{-/-} embryos of PBS treated mothers was reverted to control phenotype upon CVF treatment as visualized by immunohistochemical Cytokeratin-8 staining. The lack of *Cebpb* reactivity (indirect immunofluorescence) in *Cmas*^{-/-} embryos of PBS treated mothers was restored upon CVF treatment. PNA reactivity documenting the loss of cell surface sialylation was maintained in *Cmas*^{-/-} embryos of PBS as well as of CVF treated mothers, indicating that the asialo-phenotype was not influenced by CVF. Representative images of experiments with PBS treated mice: control n=5, *Cmas*^{-/-} n = 3 embryos; CVF treated mice: control n = 5, *Cmas*^{-/-} n = 4 embryos. (**B**) Collagen IV indirect immunofluorescence (red). Thickened Reichert's membrane (arrow) in *Cmas*^{-/-} embryos of PBS treated mothers was converted to control phenotype upon CVF treatment. Parietal endoderm marked by arrowheads. Nuclei shown in white were stained with DAPI. (**C**) Quantification of Reichert's membrane thickness measured on Collagen IV immunofluorescences at the anti-mesometrial pole (PBS: control n = 6; *Cmas*^{-/-} n = 3 embryos; CVF: control n = 5; *Cmas*^{-/-} n = 4 embryos). (**D**) Mean of fetal size as measured by the sum of areas of amniotic cavity, exocoelomic cavity, ectoplacental cavity and embryo proper in ($\mu\text{m}^2/10^5$) (PBS: control n=5; *Cmas*^{-/-} n=4 embryos; CVF: control n=5; *Cmas*^{-/-} n=3 embryos); a scheme of the areas is shown in Figure S5. Statistical analyses by ANOVA with Newman-Keuls post-test (*P < 0.05, **P < 0.01, ***p < 0.001). Error bars indicate SD (**C, D**).

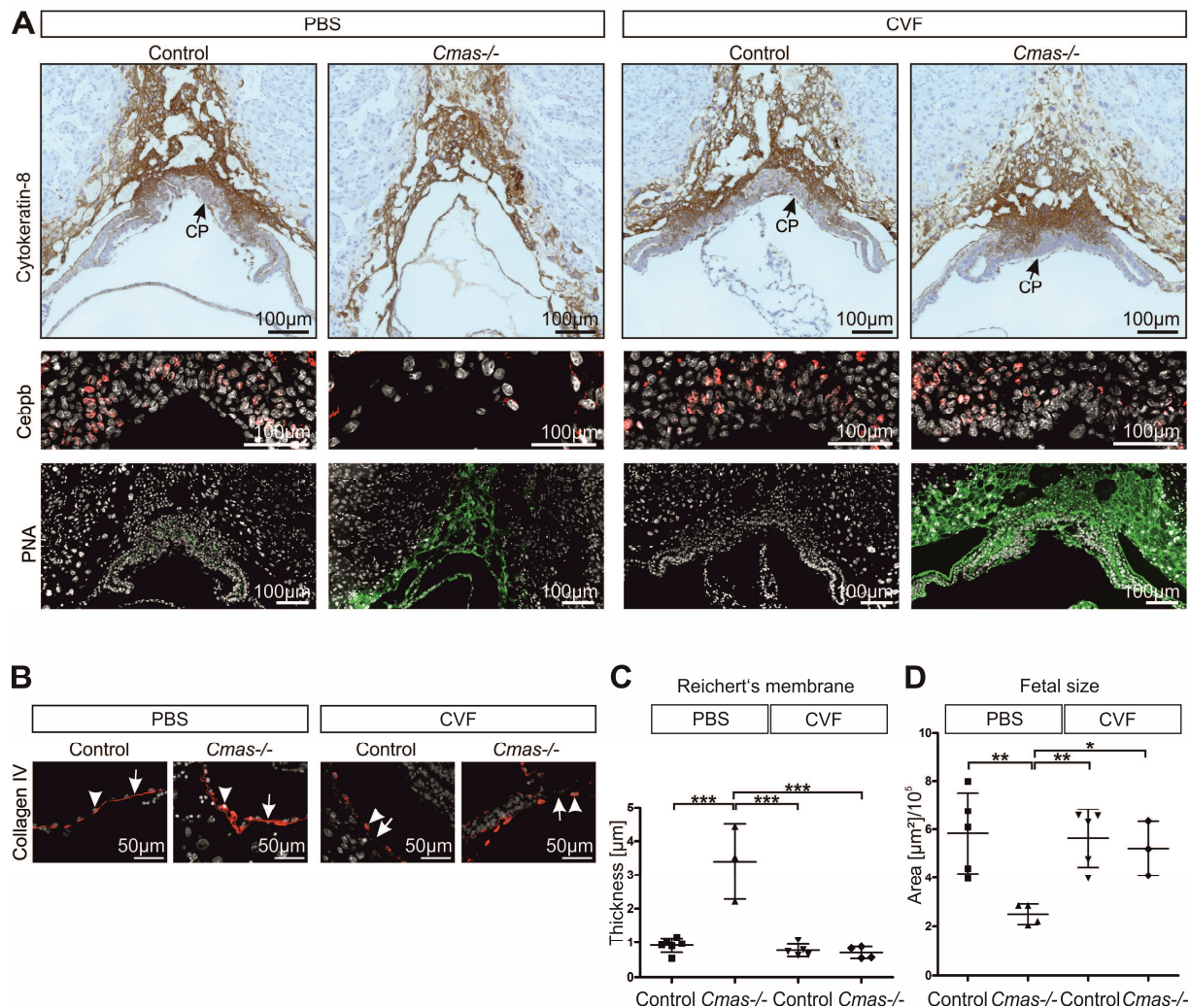


Figure 8. *Cmas*^{-/-} trophoblast cells activate the alternative pathway. Immunohistochemical analyses of complement components **(A)** C1q, **(B)** C4d, **(C)** Properdin and **(D)** C9 on sagittal paraffin-embedded sections of E8.5 embryos within the uterus. The positive C9 staining in both genotypes (upper insets) most likely reflects C9 in the fluid phase in the lumen of decidual blood vessels. Scale bars in all insets: 20 μ m. All shown experiments are representative images of control (n=12) and *Cmas*^{-/-} (n=3) embryos.

